Comparative studies of O_2 and N_2 in pure, mixed and layered CO ices

Guido W. Fuchs,*[a] Kinsuk Acharyya,[ab] Suzanne E. Bisschop,[a] Karin I. Öberg,[a] Fleur A. van Broekhuizen,[a] Helen J. Fraser,[c] Stephan Schlemmer,[d] Ewine F. van Dishoeck[a] and Harold Linnartz[a]

Received 5th December 2005, Accepted 3rd January 2006
First published as an Advance Article on the web 10th May 2006
DOI: 10.1039/b517262b

We present laboratory data on pure, layered and mixed CO and O_2 ices relevant for understanding the absence of gaseous O_2 in space. Experiments have been performed on interstellar ice analogues under ultra high vacuum conditions by molecular deposition at 14 K on a gold surface. A combination of reflection absorption infrared spectroscopy (RAIRS) and temperature programmed desorption (TPD) is used to derive spectroscopic and thermodynamic properties of the ices. It is found that for pure ices the desorption energy of O_2 is larger than that of CO and N_2. TPD spectra reveal similar desorption processes for all examined CO–O_2 ice morphologies. The different amorphous and crystalline components of pure ^{13}CO RAIR spectra are analyzed. The RAIRS data of the ^{13}CO stretching vibration show a significant difference between layered and mixed CO–O_2 ices: layered CO–O_2 ices resemble that of pure ^{13}CO whereas the spectra of mixed ices are broadened. The experiments also show that the sticking probabilities of O_2 on CO and O_2 on O_2 are close to unity. These new results are compared with recently analyzed data of CO–N_2 ices.[1,2] The differences in the TPD and RAIRS spectra of the CO–N_2 and CO–O_2 ice systems are explained by differences in quadrupole intermolecular interactions and by different crystallization processes of these ices.

1. Introduction

Studies of the chemistry in dense molecular clouds and pre-stellar cores are of interest because these systems evolve to become the early stages of planetary systems. Molecular oxygen (O_2), molecular nitrogen (N_2) and carbon monoxide (CO) are predicted to be among the most abundant small molecules in dense cores, potentially containing a significant fraction of the oxygen, nitrogen and carbon budget that is not locked up in refractory grain cores, *e.g.* in ref. 3. Direct observations of gas-phase O_2 and N_2 are difficult since these molecules lack an electric dipole moment which makes them infrared (IR) inactive and radio quiet. The abundance of gaseous N_2 can be inferred indirectly from millimetre observations of the chemically linked N_2H^+ ion which forms *via* proton transfer of H_3^+ with N_2. Such data show that in some clouds, gaseous N_2 contains a large fraction of the available nitrogen with abundances of a few times 10^{-5} with respect to H_2,[4,5] whereas the coldest and densest cores show a decrease in the gas-phase N_2 by at least a factor of two.[6] No such readily observable daughter product is available to trace O_2, however.

In contrast with N_2, O_2 has a $^3\sum$ ground state and thus a magnetic dipole moment enabling weak transitions in the (sub)millimetre range between fine-structure levels. Due to the atmospheric

[a] *Raymond and Beverly Sackler Laboratory for Astrophysics, Leiden Observatory, Leiden University, Postbus 9513, 2300 RA Leiden, The Netherlands. E-mail: fuchs@strw.leidenuniv.nl*
[b] *Centre For Space Physics, 43 Chalantika, Garia, Kolkata 720084, India*
[c] *Department of Physics, University of Strathclyde, 107 Rottenrow East, Glasgow, UK G4 ONG*
[d] *I. Physikalisches Institut, Universität zu Köln, Zülpicher Strasse 77, 50937 Köln, Germany*

opacity, $^{16}O_2$ can only be observed from space but the results from numerous attempts to detect O_2 are mostly negative. SWAS and ODIN satellite measurements have resulted in stringent upper limits on the O_2 abundance of $\leq 3 \times 10^{-7}$ and 3×10^{-6}–1×10^{-7} for cold dark clouds.[7,8] Even the recently claimed ODIN detection of O_2 at 119 GHz ($N_J = 1_1$–1_0 transition) toward ρ Oph A gives a low abundance of (0.5–6) $\times 10^{-7}$ and is still controversial.[9] Thus, the abundance of gas-phase O_2 appears to be significantly less than that of N_2. Indeed, the observed oxygen-containing molecules in the gas phase in cold clouds make up less than 10% of the available oxygen, most of it in the form of CO.[10]

Some fraction of this missing oxygen may be frozen out as solid O_2.[11] Theoretical models predict that both solid O_2 and N_2 can be important grain mantle molecules, with solid O_2 abundances as large as those of solid CO.[3,12,13] Solid CO is readily detected in cold clouds through its vibrational band at 4.67 μm (2140 cm^{-1}) with abundances up to 10^{-4}, *e.g.* in ref. 14–16. Solid O_2 has been searched for with the Infrared Space Observatory (ISO) at 6.45 μm but was not detected.[17] Indirect constraints on the amount of solid O_2 come from its influence on the shape of the absorption bands of solid CO, CO_2 or other ices. Indeed, laboratory transmission absorption spectra of mixed ices such as $CO:O_2$, $CO:N_2$ and $CO:O_2:N_2:CO_2$ show a significant broadening of the solid CO feature, *e.g.* in ref. 18 and 19. The most stringent astronomical limits come from high-quality observations of the solid CO and ^{13}CO vibrational bands which indicate that the O_2/CO and N_2/CO abundance ratios are less than unity.[15,20] These observational limits only hold for mixed ices with CO, not when O_2 or N_2 would form a separate ice layer.

The observations summarized above indicate that chemical models of dense cores need to include accurate descriptions of the processes by which O_2 and N_2 get on and off the grains. To model freeze-out and desorption, basic molecular parameters such as the sticking probabilities and binding energies are required. In addition, the kinetics of the processes need to be known. In recent years, Temperature Programmed Desorption (TPD) experiments combined with Reflection Absorption Infrared Spectroscopy (RAIRS) have become a powerful tool to determine these parameters for astrophysically relevant systems and to investigate the processes occurring in the ices upon warm-up, *e.g.* in ref. 21–24. Using our new ultra-high vacuum (UHV) set-up, we have shown that even simple ices, built from chemically closely related molecules such as CO and N_2, exhibit a complex desorption behavior.[1] The basic molecular data for the N_2–CO pure, mixed and layered ices have been summarized in a detailed study by Bisschop *et al.*[2] Here we present new experiments on the O_2–CO system, in a continued effort to understand these weakly bound systems from a chemical physics point of view and to present data to astronomers which may help to solve the mystery of the missing O_2 in clouds.[25]

The paper is organized as follows. After describing the experimental setup and the measurements procedure, results are described that have been obtained using TPD and RAIRS both for pure, mixed and layered O_2–CO ices. Estimates for sticking probabilities are derived and the experimental findings are explained in terms of the physical and chemical properties of the ices. Comparisons with the N_2–CO system are made throughout.

2. Experiment

2. 1. Experimental setup

All experiments are performed using the CRYOPAD set-up which has previously been used to study CO–N_2 ice systems.[1,2] The experimental apparatus is described in more detail in ref. 26. CRYOPAD is an ultra high vacuum setup (background pressure $\leq 1 \times 10^{-10}$ mbar) designed to study the chemical and physical interactions of interstellar ice analogs using TPD and RAIRS (Fig. 1). Ices are grown on a 2.5 × 2.5 cm^2 sample surface made out of a thin (0.1 μm) polycrystalline gold film which is coated on a copper substrate and located in the center of the vacuum chamber. The substrate is cooled by a closed-cycle He cryostat and reaches temperatures as low as 12 K. The sample temperature is monitored using two thermocouples (KP chromel *vs.* AuFe (0.07%)), one close to the Au surface and the second next to a resistive heater element. The temperature of the sample can be set from 14–300 K with a temperature accuracy better than 0.1 K using a Lakeshore 340 temperature control instrument (PDI-feedback loop). Ice growth is achieved by directing a steady molecular flow centered and perpendicular to the cold sample surface. A flow

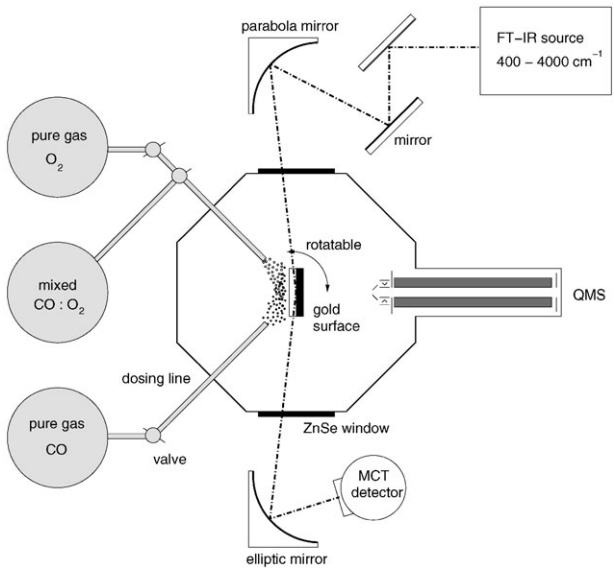

Fig. 1 Schematic view of the CRYOPAD experimental setup.

control valve ensures constant flow conditions. The details of the deposition procedure are discussed below.

The total pressure is recorded using a Bayard–Alpert-type ion gauge. At a gas exposure of around 10^{-6} mbar during one second—by definition 1 Langmuir (1 L)—and a sticking coefficient of 1, it is assumed that molecules hitting the surface build up one monolayer (1 ML). This corresponds to about 10^{15} particles cm^{-2} forming a non porous condensed solid. It is commonly assumed that interstellar ices are amorphous and the aim of any laboratory investigation should hence be to produce amorphous ice analogs. UHV conditions allow long deposition times at 10^{-8} mbar (0.01 L s^{-1}) and at low temperature, *i.e.* well below the sublimation pressure limit. Therefore, any molecule hitting the cold surface can release its excess energy to the sample well before new molecules arrive and further layers are subsequently built. Under these conditions amorphous, non-crystalline, ice is expected to grow.

Once ices are built their desorption behavior is examined using TPD, *i.e.* CO and O_2 molecules are released from the surface during a controlled linear temperature rise from 14 to 80 K at a heating rate of 0.1 K min^{-1} and monitored using a quadrupole mass spectrometer (QMS, Pfeiffer Prisma). A thoriated iridium filament is used in the QMS ion source for ionization.† Complementary to TPD, RAIRS is applied to examine the solid ice phase. RAIR spectra are not identical to transmission spectra due to the "surface selection rule"; in RAIRS only the radiation component which is due to a dipole oriented perpendicular to the sample surface can be observed.[27] Nevertheless, changes and trends which occur during the warming up phase prior to desorption can be recorded and valuable information on new or restructured binding sites, phase-changes and estimates of remaining layer thicknesses is obtained. The spectra are recorded using a Fourier Transform IR spectrometer (BioRad, Excalibur FT3000) between 400–4000 cm^{-1}, *i.e.* between 2.5 and 25 μm. The IR beam is guided into the vacuum chamber by standard optics through a ZnSe window, subsequently reflected at the ice/gold substrate under a grazing angle of 6° and focused onto a mercury–cadmium–telluride detector. The sensitivity of the setup with respect to the ^{13}CO

† For most experiments the filament worked reliably but in a few cases, see Fig. 2g and h, a shoulder developed between 27 and 29 K which is an experimental artifact. After a filament change, subsequent experiments as well as control $^{12}CO/^{16}O_2$ experiments showed no shoulder at this temperature for this and other ice structures.

stretching vibration at 2095 cm^{-1} is such that it can detect 0.1 to 0.01 ML of CO condensed on the surface, *i.e.* 10^{13}–10^{14} molecules cm^{-2}.[26]

2.2 Ice morphologies and measurement procedure

^{13}CO isotopomers (Cambridge Isotopes, Inc. 99%) are used to obtain RAIR spectra which can be compared directly to the previously taken $^{15}N_2$–^{13}CO data.[2] $^{18}O_2$ isotopomers (Icon Isotopes, 99%) are used to distinguish oxygen atoms that originate either from O_2 or from $^{13}C^{16}O$ in the TPD spectra following fragmentation in the ionization chamber of the QMS. This enables monitoring of the total oxygen budget $0.5 \times n(O^+) + n(O_2^+)$. The m/z values of 36 ($^{18}O_2$), 29 ($^{13}C^{16}O$), 18 (^{18}O), 16 (^{16}O) and 13 (^{13}C) are recorded simultaneously. To check for contaminations like CO_2, $^{16}O_2$, $^{14}N_2$, and H_2 also m/z = 44, 32, 28, and 2 values are monitored. During all experiments the purity of the deposited gases was found to be better than 99%. The desorption behavior, as reflected in the TPD spectra, of $^{18}O_2$ and $^{16}O_2$ as well as of ^{13}CO and ^{12}CO is identical whereas the RAIR spectra differ by the usual isotope effect, *i.e.* the stretching vibration of ^{12}CO is around 2140 cm^{-1} and that of ^{13}CO is around 2093 cm^{-1}.

All the CO–O_2 gas mixtures are pre-prepared and subsequently connected to the gas-dosing system of the UHV chamber. The sample is cooled down to 12 K and then flash-heated up to 200 K to release any residual gas from the sample surface prior to deposition. The same gas dose (mbar × s) previously set at room temperature is then used for the deposition of the molecules at 14 K. The achieved layer thickness of the ice is assumed to be linear to the gas exposure time (deviations from this assumption are discussed in ref. 2). A RAIR background spectrum is taken prior to deposition and subsequently used for all further data reduction of the sample spectra. The ice is slowly warmed up at a rate of 0.1 K min^{-1} to 80 K and the desorbed gases are monitored by a QMS. At 14 temperature positions between 15.5 K and 38.5 K RAIR spectra are taken at a 0.5 cm^{-1} resolution using 128 scan averages ($\approx$ 4 min integration time).

Studies of ice systems like CO–CO_2 and CO–N_2 have shown that the morphology of the ice, *i.e.* whether CO is mixed or separated as a layer, is crucial for the IR absorption profile.[2,28] Most transmission experiments have been performed using thick layers of ices of around 0.1–0.5 μm, corresponding to 180–900 monolayers of α-crystalline CO (assuming a lattice parameter a = 5.65 Å at 20 K). Astrophysical observations of young stellar objects in nearby low-mass star forming clouds indicate that a large fraction of the CO ice exists in a nearly pure form at thicknesses of around 40 monolayers.[15] The RAIRS studies presented here use thin (20–80 monolayers), astrophysically relevant ice thicknesses of pure, layered and mixed ices. Below 40 L, layer growth of CO ice is hindered by non-uniform, so-called island growth, and only above 40 L a substrate-independent behavior of co-adsorbed species is expected. Consequently, the total ice thickness of CO–O_2 ices is chosen to be larger than 20 L and is typically around 80 L. Astrochemical models suggest that atomic oxygen and nitrogen are transformed into molecular form at later times and higher extinctions compared to the atomic carbon conversion into the CO molecule.[12,29,30] This would imply that O_2 or N_2 freeze out onto a pre-existing CO layer. Thus, mixed ices or layered ices of O_2 onto CO seem to be the most realistic scenarios in interstellar space and these structures are prepared in the present experiments. Table 1 gives an overview of the newly studied CO–O_2 ices and also summarizes the CO–N_2 data used in this work for comparison.

3. Data analysis and results

3.1 TPD

In the next sections TPD results for pure, mixed and layered O_2 and CO ices are presented and a comparison with the CO–N_2 ice system is given (Fig. 2).

3.1.1 Pure ices. The desorption behavior of pure-O_2 and CO is shown in Fig. 2a and 2e for 20 L, 40 L and 80 L exposures. In contrast to N_2, O_2 desorbs at higher temperatures than found for CO. As a 'rule of thumb' the desorption energy E_d can be estimated from the peak temperatures of N_2, CO and O_2 using (see ref. 31 p. 72, 1 kJ mol^{-1} $\simeq$ 120.272 K)

$$E_d[K] = T_{peak}[K] \times 30.068. \quad (1)$$

Table 1 Overview of ice morphologies and ice exposures for the CO–O_2 experiments

	^{13}CO/L	$^{18}O_2$/L	$^{15}N_2$/L	Total/L
Pure CO	20, 40, 80	—		Same
Pure O_2	—	20, 40, 80		Same
Pure N_2[a]	—		20, 40, 80	Same
CO : O_2 mixed (1 : 1)	40	40		80
CO/O_2 layered	40	40		80
O_2/CO layered	40	40		80
CO : N_2 mixed (1 : 1)[a]	40		40	80
CO/N_2 layered[a]	40		40	80
N_2/CO layered[a]	40		40	80

[a] See ref. 1 and 2. X/Y stands for layered ices where the X species is on top of the Y species. X : Y stands for X mixed with Y.

Thus for 40 L ices $T_p(N_2) = 26.4$ K, $T_p(CO) = 28.5$ K and $T_p(O_2) = 30.9$ K result in $E_d(N_2) \approx 790$ K, $E_d(CO) \approx 855$ K and $E_d(O_2) \approx 930$ K. The order of desorption for all three species is expected to be zero, *i.e.* the TPD spectra reveal a common leading edge for different exposures and a shift to higher peak temperatures with increasing layer thicknesses. However, due to inhomogeneous ice growth particularly at lower thicknesses, a 0th-order desorption can only be verified from 40 L upwards for CO and O_2 ices and remains doubtful for N_2 ices.[2] In a 0th-order process the desorption rate $r_d(T)$ should be independent of the amount of adsorbates (CO, O_2, N_2) on the surface and is expressed using a Polanyi–Wigner type equation

$$r_d(T) \equiv \frac{dN_{gas}}{dt} = \nu_0 e^{-E_d/T} \quad (2)$$

with ν_0 the pre-exponential factor for 0th-order (around 7×10^{26} molecules cm^{-2} s^{-1}), T the ice temperature, and N_{gas} the number of desorbed gas phase molecules per cm^2. The ion count of the QMS is assumed to be proportional to N_{gas} and ν_0 can be viewed as the product of the molecular vibrational frequency and the surface density of molecules (*i.e.* in an ideal solid of 10^{15} molecules cm^{-2}). By fitting the leading edge of several TPD spectra of ices of different thicknesses the pre-exponential factor and E_d are determined more accurately (Table 2). As expected, for each of the molecules the desorption energy E_d is between the sublimation enthalpy $\Delta H_{sub,T_b}$ at the boiling point and the theoretical sublimation point $\Delta H_{sub,T=0K}$ at $T = 0$. The reproducibility of the TPD spectra in terms of the temperature peak position is better than 0.2 K. If the enthalpy of adsorption and desorption are equal in these systems, the desorption energies E_d are equivalent to the adsorbate-surface binding energy E_b.

3.1.2 Mixed ices. CO–O_2 ices: The TPD spectra of CO and O_2 (Fig. 2b) resemble the pure CO and O_2 spectra with the exception that the CO peak temperature increases by 0.5 K and the O_2 peak decreases by 0.5 K. Codesorption of CO with O_2 is not observed. From ongoing experiments for a series of ice thicknesses (data not presented here,[25]) a similar common change of binding environments is seen which shifts the binding energies toward each other by equal, but small amounts. Intimately mixed O_2 and CO cannot interact well with each other, probably because O_2 has zero dipole moment and only a small quadrupole moment (Table 3). Therefore, the desorption process happens rather independently. At lower coverage (not shown here) segregation can play a more dominant role.

CO–N_2 ices: In the CO : N_2 system (Fig. 2f) the CO desorption peak is shifted to higher temperatures and broadened with respect to the pure-CO spectrum. This suggests a hindered desorption due to the presence of N_2. The N_2 spectrum is also broader than in pure-N_2 ice (not shown) and the desorption peak shifts to a higher temperature. Roughly half of the N_2 is estimated to codesorb with CO, *i.e.* from N_2-CO-like binding sites, whereas the other half desorbs at lower temperatures presumably from similar environments as seen in the pure-N_2 TPD spectra, *i.e.* from N_2–N_2 binding sites.

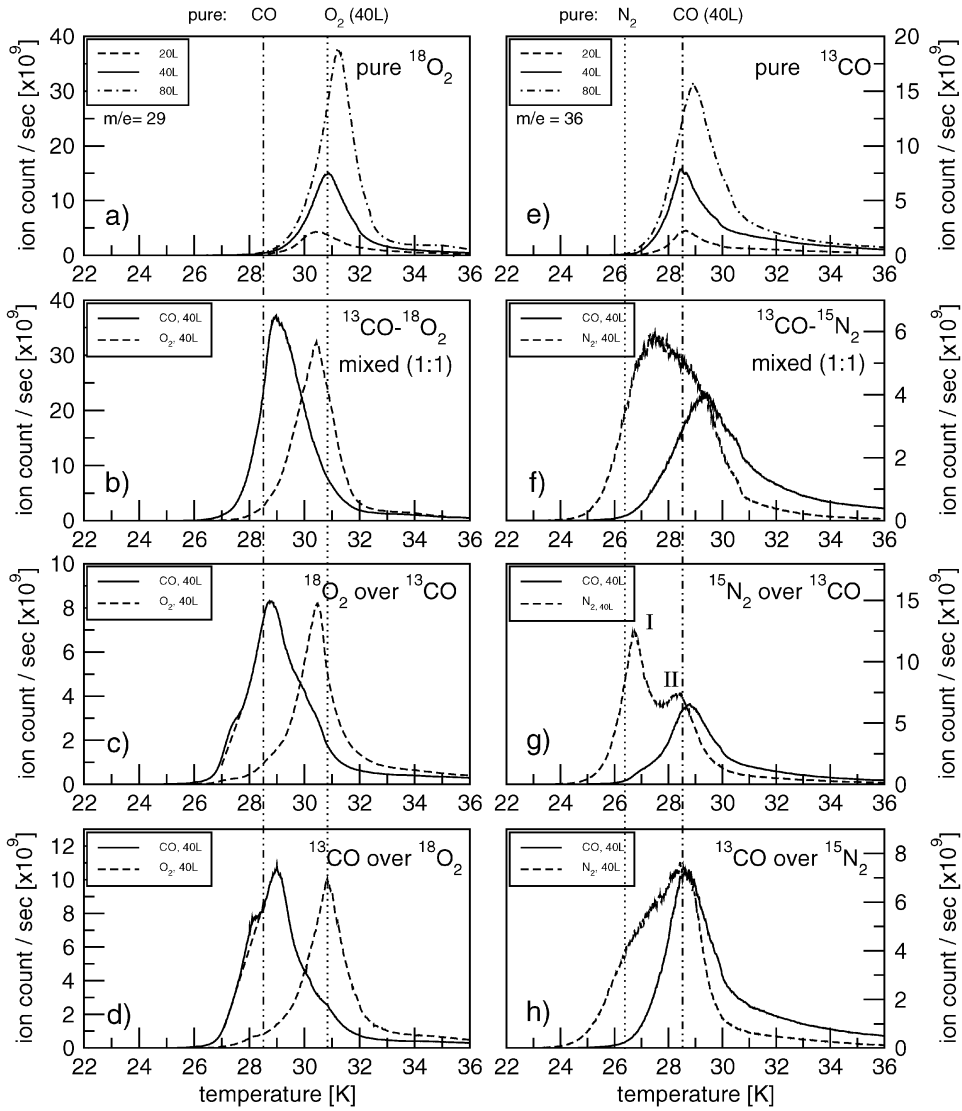

Fig. 2 TPD spectra of pure, mixed and layered $^{18}O_2$, ^{13}CO, and $^{15}N_2$. (a) pure O_2 ices at thicknesses of 20 L, 40 L, and 80 L; (b) equimolar mixed CO : O_2 ice; (c) layered structure of O_2 over CO; (d) CO/O_2 ice; (e) pure CO ices at thicknesses of 20 L, 40 L, and 80 L; (f) equimolar mixed CO : N_2; (g) layered structure of N_2 over CO; (h) CO/N_2 ice. In all graphs vertical lines have been superposed to indicate the peak temperature of desorption for pure-CO (dashed-dot) at 28.5 K (40 L) and pure-N_2 (dotted) at 26.4 K (40 L) or pure-O_2 (dotted) at 30.9 K (40 L). The shoulders at 27 K and 27.8 K in Fig. (g) and (h) are experimental artifacts (see text) and the dashed lines indicate the expected curvature at these points. Count rates can vary over time and differ from species to species. For the O_2 measurements a different filament in the QMS has been used. For all spectra the heating rate is 0.1 K min^{-1}. Plots (f), (g), and (h) are taken from ref. 1.

The main difference between CO : O_2 and CO : N_2 mixtures is that the CO : O_2 does not show any significant broadening in the TPD spectrum compared with the pure ices. This is probably due to the different strengths of the intermolecular interactions of CO–O_2 and CO–N_2. Contrary to CO and O_2, CO and N_2 can interact easily due to quadrupole interactions and the broadening effect may therefore be due to a wide range of binding environments in a mixed CO : N_2 ice. In addition,

Table 2 Desorption parameters for pure ices compared with sublimation enthalpies ΔH

	ν_0/cm^{-2} s^{-1}	[K]	E_d/kJ mol^{-1}	$\Delta H_{sub,T_b}$/kJ mol^{-1}	$\Delta H_{sub,T=0K}$/kJ mol^{-}
^{13}CO	$7 \times 10^{26\pm1}$	855 ± 25	7.11 ± 0.2	6.87 (^{12}CO)[c]	7.942 (^{12}CO)[d]
$^{15}N_2$[af]	$7 \times 10^{26\pm1}$[b]	790 ± 25	6.57 ± 0.2		7.005 ($^{15}N_2$)[d]
				6.28 ($^{14}N_2$)[c]	6.954 ($^{14}N_2$)[d]
$^{18}O_2$	$7 \times 10^{26\pm1}$[b]	925 ± 25	7.69 ± 0.2	7.26 ($^{16}O_2$)[c]	8.665 ($^{16}O_2$)[e]

[a] Data from ref. 1. [b] Fixed to CO value. [c] $\Delta H_{sub} = \Delta H_{vap,T_b} + \Delta H_{fus,T_{l-s}}$ from ref. 39 with $\Delta H_{vap,T_b}$ the enthalpy of vaporization at the boiling temperature T_b and $\Delta H_{fus,T_{l-s}}$ the enthalpy of fusion at the solid–liquid transition temperature T_{l-s}. [d] Ref. 40. [e] Ref. 41. [f] Ref. 2 gives parameters for 1st-order desorption.

during warm-up in a TPD experiment, differences in crystallization of a N_2–CO ice *vs.* O_2–CO ice may play a role, see Section 3.2.2

3.1.3 Layered ices. CO-O_2 ices

O_2 on top of CO. Fig. 2c shows a TPD spectrum of an equimolar layered O_2 on top of CO ice. The CO trace peaks at a slightly higher temperature than pure CO and has a weak shoulder at the desorption temperature of O_2 around 30–31 K. As in the case of mixed CO : O_2 the peak temperature for O_2 is shifted towards a lower temperature with respect to pure O_2. This is a systematic effect which has been examined by looking at ices with different thicknesses.

CO on top of O_2. Fig. 2d depicts the TPD spectra of CO on top of O_2. Also here the CO peak is shifted towards higher temperatures with respect to a pure-CO ice desorption and has a weak shoulder at 30–31 K. The O_2 temperature peak is at the same position as seen for the pure O_2 ice. This seems to be a general trend also for other ice thicknesses.

CO–N_2 ices

N_2 on top of CO. Fig. 2g shows that the N_2 trace has two distinct peaks at 26.7 K (peak I) and 28.4 K (peak II). Peak I appears close to the temperature at which pure N_2 desorbs, whereas peak II, is close to the CO desorption peak. The CO desorption peak is close to that found for pure-CO ice. The ratio between the height h_i of peak I and II in Fig. 2c is a function of the thickness of the ice and for small thickness h_I/h_{II} can be as low as 0.35 whereas at large thickness it is larger than 1.6. The turn-over point is around 40 L–60 L.

CO on top of N_2. The N_2 trace in Fig. 2h is broadened due to two components similar to peak I and II in Fig. 2c, whereas the CO trace peaks at the same temperature as where pure CO ice desorbs. The ratio h_I/h_{II} again depends on thickness, but the turnover point $h_I/h_{II} = 1$ is at higher thickness ($\approx$ 80 L).

The appearance of two separate peaks in both morphologies, *i.e.* N_2 on top of CO and CO over N_2, can be understood by assuming a mixing process followed by a re-segregation process.[2] The diffusion process mixes the N_2 and CO layers from 20 K onwards. At 25–26 K the nitrogen molecules from pure-N_2 sites desorb and at higher temperatures only N_2 at N_2–CO binding sites will be left to desorb. Since diffusion and segregation have different barrier energies ($E_{diff} < E_{segr}$), ices of different thickness and layer structure behave differently. The competition between diffusion and desorption at 26–28 K for N_2 results in different peak I heights for different ice thicknesses and the subsequent segregation process can only build upon the available intermixed N_2 (to CO) molecules. The fact that diffusion and desorption follow different kinetic orders, with the 1st-order desorption process depending on the available mixed molecules, is the cause for the thickness dependence of the peak I to peak II height ratio.

The main difference between the CO–O_2 and CO–N_2 ices is that no strong feature indicative of CO–O_2 binding is found: neither the pronounced peak II seen for the N_2/CO ice nor the low-temperature shoulder of N_2 seen in CO/N_2 ice is observed in layered CO–O_2 ices. Since CO is more volatile than O_2 and N_2 is more volatile than CO a comparison between Fig. 2g and Fig. 2d is the appropriate choice. Here the most striking difference is the reversal of the peak-to-shoulder relation for the O_2/CO and CO/N_2 system. CO in O_2/CO desorbs close to the pure CO desorption temperature, whereas N_2 in CO/N_2 has a significant amount of N_2 molecules codesorbing with CO. The equivalent CO/O_2 ice system for nitrogen is N_2/CO (compare Fig. 2c with 2h), which

behave similarly for the first desorption peaks of N_2 and CO. The codesorption of O_2 with CO is strongly suppressed in the CO/O_2 ice but existent. In general, the spectra of layered CO/N_2 and CO/O_2 reveal that O_2 does interact with CO but to a far lesser extent than N_2 does. In all cases, O_2 and CO desorption do not influence each other much and resemble the pure ices.

3.2. RAIRS

RAIRS is a valuable technique to understand processes within the ice that cannot easily be inferred from TPD data. RAIR spectroscopy is more sensitive than transmission spectroscopy and thus well suited for investigations of thin ices. As discussed in Section 2.1, spectra of RAIRS and transmission spectroscopy can be different for the same ice.

3.2.1 Pure ices. Fig. 3 shows the RAIR spectra of a pure ^{13}CO ice (40 L thickness). At least four different peaks can be distinguished for the ^{13}CO stretching vibrational band. Their heights, widths and positions change with temperature, thus indicating structural changes in the ice. It is known that multilayered α-CO crystals reveal a splitting in the CO-stretching vibrational mode, *i.e.* a LO-TO splitting of around 4 cm^{-1}, *e.g.* in ref. 32 and 33. Peak 4 at 2091.5 cm^{-1} is at the frequency position of the transversal optical (TO) component of α-crystalline CO and peak 3 at 2095.1 cm^{-1} at the longitudinal optical (LO) mode. Peak 2 at 2096.1 cm^{-1} is due to amorphous CO ice. The origin of peak 1 at 2097.6 cm^{-1} is not clear but may also be due to amorphous ice.

From the deposition temperature at 14 K up to 26 K peak 2 of the amorphous CO is the most dominant feature and peak 1 develops from a shoulder-like feature of peak 2 to a well separated peak from 26 K onwards. Peak 1 remains at the same frequency from the deposition temperature until the desorption temperature. At $T_{jump} = 27$ K peak 3 starts to dominate the spectra and only vanishes when all the molecules have been desorbed. The observed line profiles caused by the RAIRS technique are not symmetric, *e.g.* not Gaussian. The width (FWHM) of peak 1 + 2 at low temperatures is around 2.3 cm^{-1} and peak 3 has a FWHM of 1.3 cm^{-1} at 28.5 K.

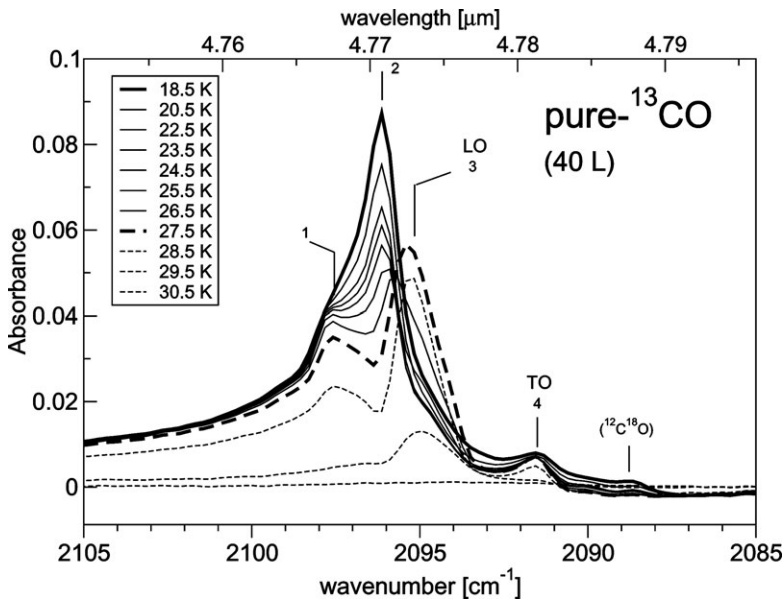

Fig. 3 RAIR spectra of ^{13}CO during a TPD experiment. Peaks appear at (1) 2097.6 cm^{-1}, (2) 2096.1 cm^{-1}, (3) 2095.1 cm^{-1} (LO), and (4) 2091.5 cm^{-1} (TO). At low temperatures a single peak at 2096 cm^{-1} of amorphous ^{13}CO dominates the spectrum whereas at temperatures close to the desorption temperature the α-crystalline LO-component at 2095.1 cm^{-1} and a peak at 2097.6 cm^{-1} are well pronounced. The feature at 2088.8 cm^{-1} is due to $^{12}C^{18}O$. For clarity, the individual spectra of the graph have been off-set to have equal absorbance at 2080 cm^{-1}.

The intensity of the LO and TO components depends on the polarization of the electromagnetic field and light polarized perpendicular (p-polarized) to the surface shows both the LO and TO components.[33] RAIR spectra with light polarized perpendicular (p-polarized) to the surface have a more intense LO component than TO component, as in our experiment. In general the ratio of the LO and TO peaks is a rather complicated function of the angle of incidence of the light and the ice thickness. The TO component varies little with temperature, whereas the LO feature undergoes significant change.

The appearance of LO-TO modes in α-CO crystals can be understood as follows. In bulk CO ice the infrared active F-mode is threefold degenerate in the isotropic infinite sized cubic crystal and therefore results in a single vibrational feature.[33] Fox & Hexter were the first to notice that the crystal shape can lower the symmetry and lift degeneracies.[34] A thin slab with the short dimension L less than the wavelength λ of the electromagnetic field and the long dimensions of the crystal longer than λ can cause a LO-TO splitting $\Delta\nu_{\text{LO-TO}}$. This splitting is due to vibron–phonon combination modes and can be investigated by vibron theory, *e.g.* assuming dipole–dipole interaction. For α-CO $\Delta\nu_{\text{LO-TO}}$ is calculated to be between 4–5 cm^{-1} with only minor differences between ordered and disordered crystals.[32,33] Zumofen concludes that the LO-TO splitting is nearly exclusively based on a dipole–dipole interaction.[32] Palumbo *et al.* note that amorphous ice has a LO-TO splitting too, but they do not find any direct relation of the LO-TO splitting to the morphology.[35] Thus, they assume amorphous ice to have the same LO frequency as crystalline ice. We performed additional experiments (not shown here) to investigate the difference in RAIR spectra between amorphous and crystalline ices and conclude that the 2096.1 cm^{-1} feature is the LO component of amorphous CO ice.[36] An ice thickness dependence of the RAIR spectra has to be considered as well but is not further discussed here, see ref. 35. The change from peak 2 to 3 is then due to a phase change from amorphous to crystalline ice close to the desorption temperature. Thus, the amorphous CO ice can be assumed to have a relatively closed packed structure which allows for dipole–dipole interactions with an $\Delta\nu_{\text{LO-TO}}(^{13}\text{CO}) \approx 4.6\ \text{cm}^{-1}$. No clear LO-TO splitting has yet been observed in space but first attempts are discussed in Pontoppidan *et al.*[15] In the future, models to extract optical constants from RAIR spectra may help significantly to provide data for the astronomical community.[37]

Trace amounts of other isotopic species like ^{12}CO (or $^{13}\text{C}^{18}\text{O}$ at 2040 cm^{-1}) are visible in the RAIR spectra of our ices which can give information about the local environment due to their linewidth and position. In the ^{13}CO ice, ^{12}CO cannot dipole–dipole interact and thus cannot build up LO and TO modes. Indeed, the ^{12}CO feature is a single peak at $\bar{\nu}(^{12}\text{CO}) = 2140\ \text{cm}^{-1}$ which besides the decrease of signal strength above 29 K due to desorption does not show any change in its line shape at 27 K. Thus the introduction of impurities of isotopic species in the main ice can serve as a valuable tool to circumvent the vibron–phonon coupling. The ^{12}CO line in the ^{13}CO ice has a width of 1.5 cm^{-1}. The complementary experiment where ^{13}CO is at a 1% level in a pure ^{12}CO ice results in a single peak at $\bar{\nu}(^{13}\text{CO}) = 2092.5 \pm 0.2\ \text{cm}^{-1}$, consistent with $\bar{\nu}(^{13}\text{CO}) = 2092.2\ \text{cm}^{-1}$ as reported by Chang *et al.*[33] Contrary to the ^{12}CO feature which lies nearly at the mean value of the LO and TO components, the ^{13}CO feature is much closer to the TO component.

3.2.2 Mixed ices. CO–O_2 ices

The $\text{CO}:\text{O}_2$ mixed ice has its main peak at 2094.7 cm^{-1} with a FWHM of 4 cm^{-1} at low temperatures. This peak abruptly shifts to 2095.5 cm^{-1} between 24.5 and 25.5 K (Fig. 2d). In the RAIR spectra of pure CO a similar behavior is seen at 27 K from 2096.1 to 2095.1 cm^{-1}. Compared with peak 2 of pure CO a red shift between 0.6 and 1.4 cm^{-1} is observed. The transmission spectra of ^{12}CO at 10 K reported by Ehrenfreund *et al.* have a red shift with respect to $\bar{\nu}(^{12}\text{CO})$ of 1.4 and 1.1 cm^{-1} in a $^{12}\text{CO}:{}^{16}\text{O}_2$ (1 : 0.7) and (2 : 1) mixture, respectively.[18] They observe linewidths of 5.2 cm^{-1} (1 : 0.7 mix) and 3.8 cm^{-1} (2 : 1 mix). Our weak trace ^{12}CO feature in the 1 : 1 $^{13}\text{CO}:\text{O}_2$ mixed ice below 25 K is at 2139.2 cm^{-1} and changes for higher temperatures to 2139.8 cm^{-1}, *i.e.* close to $\bar{\nu}(^{12}\text{CO})$. The linewidth changes from 3.9 cm^{-1} at low temperatures to 1.8 cm^{-1} above 25 K. The broad linewidth at low temperature is due to a variety of different binding sites as is commonly seen in mixtures. The change of the linewidth at 25 K indicates a more homogeneous environment of at least CO, *e.g.* micro-crystals of CO surrounded by O_2.

The RAIR spectrum of $\text{CO}:\text{O}_2$ is explained as follows. Since for pure CO a phase change from amorphous to crystalline structure is seen at higher temperatures, *i.e.* at 27 K, the observed

Table 3 Basic properties of α-crystalline CO, N_2 and O_2

	Dipole[a] μ/D	Quadrupole moment[c] $Q/10^{-26}$ esu	$T_{\alpha-\beta}$ ($p = 0$)[ab] /K	Crystalline structure/symmetry[ab]
$^{12}C^{16}O$	0.112	2.5	61.6	N_2-type/$P2_13$
$^{14}N_2$	—	1.4	35.6	N_2-type/$P2_13$
$^{16}O_2$	—	0.4	23.9	O_2-type/$C2/m$

[a] Ref. 40. [b] Ref. 41. [c] Ref. 42.

frequency shift at 25 K in the mixed ice may be due to a crystallization of CO induced by a phase change of O_2. The basic properties of crystalline O_2, CO and N_2 ices are summarized in Table 3. Solid O_2 in its α-phase is orientationally ordered, has a base-centered structure and a transition temperature $T_{\alpha-\beta}(^{16}O_2)$ as low as 23.9 K. The β phase of solid O_2 has a rhombohedral lattice structure which could cause severe steric effects as seen in the RAIR spectrum for CO–O_2 mixed ice. A micro crystallization of O_2 at least in its α-form seems likely within our investigated temperature range between 15 and 30 K. It is not clear whether the observed redshift of mixed CO : O_2 is due to α-O_2 at temperatures below 25 K, but a β-phase O_2 is likely to cause a segregation of O_2 and CO on the microscopic scale due to different crystal structures from 24 K onwards. In that case CO molecules would still see an inhomogeneous environment, but to a lesser extent. This explains the reduced broadening of the ^{12}CO band profile within the ^{13}CO ice. Due to the small amount of material deposited and the weakness of the band at 1551 cm^{-1} no feature of pure O_2 could be observed in the RAIRS and there is no further information in which form O_2 molecules were present in the ice.

CO–N_2 ices

In the $^{13}CO : N_2$ mixed ice the main peak appears at 2095.2 cm^{-1} with a FWHM of 4 cm^{-1} and after a small change in linewidth around 20 K remains fixed during warm up until all molecules have desorbed (Fig. 2e). This peak is redshifted relative to peak 2 of the pure CO ice by $\sim$0.9 cm^{-1}. In their transmission spectra Elsila *et al.* find that N_2 causes a redshift of 1.3 cm^{-1} with respect to $\bar{\nu}(^{12}CO)$ with a width of 2.6 cm^{-1} when using a 1 : 2 CO : N_2 mix.[19] No shift in our weak trace ^{12}CO feature was detected in the 1 : 1 $^{13}CO : N_2$ mixed ice, *i.e.* the peak appeared at $\bar{\nu}(^{12}CO)$ of pure CO, with a linewidth of $\sim$2.5 cm^{-1} consistent with ref. 19.

The CO : N_2 RAIRS show a peak frequency of the CO band close to that of the LO component of α-crystalline CO. N_2 and CO have the same α-crystalline structure at low temperatures, *i.e.* below $T = 35.6$ K, see Table 3. Assuming that N_2 crystallizes around 15–20 K, CO may be already in a co-crystalline form from 20 K onwards, thus explaining the center frequency to be at the LO position of α-crystalline CO. The line width is in accordance with that of a co-crystallized ice.

The most obvious difference between the CO : O_2 and CO : N_2 RAIRS is the sudden shift around 25 K in the spectrum of CO : O_2 which is not seen in the CO : N_2 ice. This is likely caused by the different crystalline structure of O_2 compared with CO and N_2.

3.2.3 Layered ices. CO–O_2 ices: At first sight the stretching vibration of ^{13}CO in a O_2/CO ice resembles that of pure CO (Fig. 2b). At low temperatures the main peak is around 2096.3 cm^{-1} and besides a weak TO component at 2091.7 cm^{-1} there are no further features. As in the case of pure CO the TO component stays constant over time. The development of a shoulder which further grows to a peak towards 2097.6 cm^{-1} from 26 K onwards is also similar to the pure CO spectra as well as the LO component which builds up around 28 K. This is expected, since for O_2 and CO no mixing is observed, and hence, any effect of O_2 crystallization should not influence the CO structure.

CO–N_2 ices: The layered N_2/CO ice RAIR spectrum resembles that of O_2/CO over wide parts (Fig. 4c). However, a remarkable difference is seen between 20 K and 27 K when a wing of constant intensity builds up between 2093 and 2095 cm^{-1}. In Fig. 4c this wing appears at 24 K, but the intensity plot (not shown) reveals that it starts already around 20 K. The integrated absorbance of this feature lies between 12–20% of the total CO absorbance. The weak spectral feature at 2140 cm^{-1} due to trace amounts of ^{12}CO does not show any frequency shift at 20 K nor after

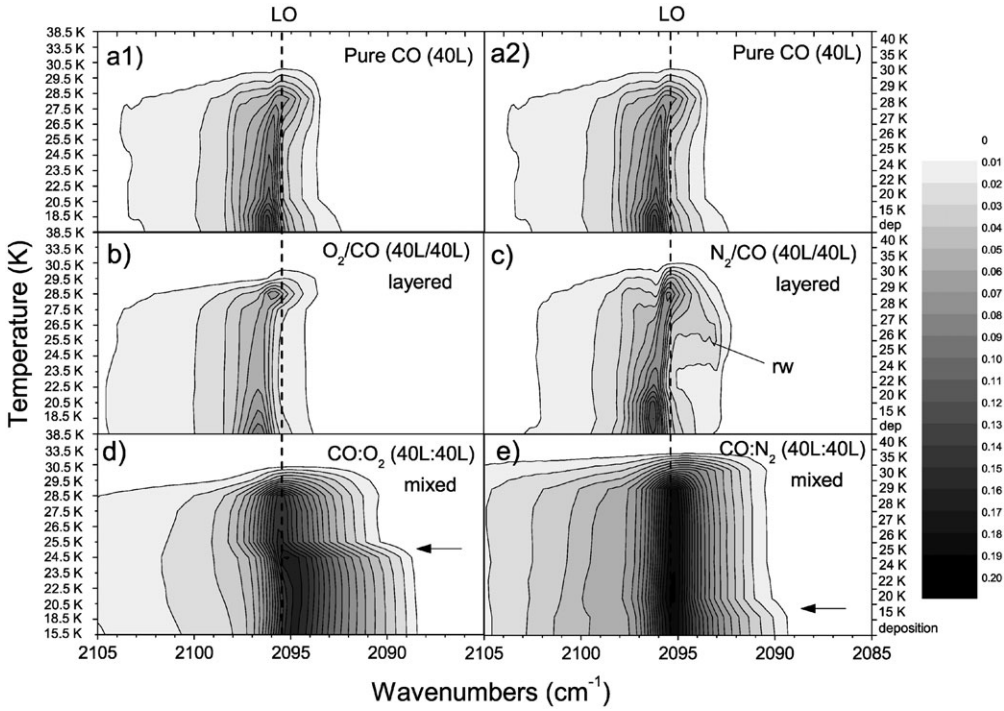

Fig. 4 2-D RAIR spectra of the stretching vibration of ^{13}CO for pure-^{13}CO, N_2 : CO mixtures, N_2/CO layers and O_2/CO ices mixed and layered. The ordinate is a non-linear temperature scale. For all graphs the ^{13}CO exposure was 40 L. The total gas exposure CO + N_2 or CO + O_2 for (b)–(e) is 80 L. The LO frequency of α-crystalline CO is indicated by a vertical dashed line (LO). Fig. a1 and a2 are 2-D plots from Fig. 3. The red wing feature for layered N_2/CO is indicated by (rw) and the frequency shifts for the mixed ices are marked with an arrow.

27 K, nor does the linewidth change ($\Delta\nu \sim 1.5$ cm^{-1}). The widths of ^{13}CO in both the O_2/CO and N_2/CO ices are very close to that of pure CO ice.

This finding supports a model of layered N_2/CO TPD data with a mixing process between N_2 and CO starting at 20 K up to 27 K. If the mixing process happens systematically with higher mixing concentrations at the interface between CO and N_2 then the N_2/CO RAIR spectra can be explained as follows. N_2 may be already crystallized when the diffusion process starts at 20 K. Mixing of N_2 into the CO ice causes different binding sites for a certain fraction of the CO ice. In this case the change of linewidth of the ^{12}CO feature in the ^{13}CO ice between 20 and 27 K is expected to be between 12 to 20% of $\Delta\nu_{mix} - \Delta\nu_{pure}$, *i.e.* 0.1 and 0.2 cm^{-1}, which is consistent with the observed constant linewidth. Parts of the CO ice will still be pure amorphous ice. CO crystallization ends this process at around 27 K and the typical LO component of α-CO is seen: since in the diffusion model CO is never fully mixed with N_2 a shift in the ^{13}CO feature at 27 K is still expected and also observed.

Thus, the main difference between the O_2/CO and N_2/CO RAIRS is the red wing feature at 20–27 K between 2093 and 2095 cm^{-1} which is only seen for the N_2/CO ice. It indicates a mixing process which is not evident for CO–O_2 ices.

3.3 Sticking probability

Our experimental setup does not allow a direct measurement of sticking coefficients S with the accuracies as can be achieved by molecular beam facilities. Nevertheless, lower limits on the sticking coefficients can be estimated by comparing the gas load N_x^c of species x reaching the mass

Table 4 Estimated sticking coefficients (lower limits)

System	Sticking probability	Temperature/K
$CO \rightarrow CO$	$\geq 0.9 \pm 0.05^a$	14
$N_2 \rightarrow N_2$	$\geq 0.85 \pm 0.05^a$	14
$N_2 \rightarrow CO$	$\geq 0.87 \pm 0.05^a$	14
$O_2 \rightarrow O_2$	$\geq 0.87 \pm 0.05$	15.5
$O_2 \rightarrow CO$	$\geq 0.87 \pm 0.1^b$	15.5
$CO \rightarrow O_2$	$\geq 0.95^{+0.05b}_{-0.1}$	15.5

[a] Data from ref. 2. [b] Averaged value valid within first 3 monolayers.

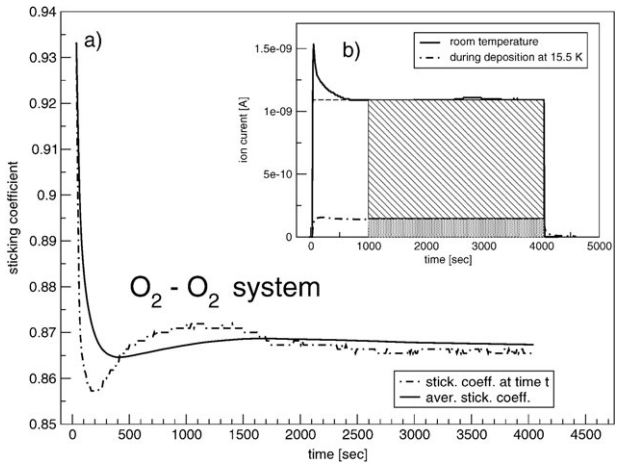

Fig. 5 Measured sticking probability of O_2 on gold and O_2. Plot (a) shows the sticking probability of O_2 molecules exposed to a gold surface over a time of 4000 s. Here, 100 s are assumed to correspond to one monolayer. Initially the sticking coefficient drops rapidly from 0.93 to 0.87 until a coverage of 4–5 monolayers O_2 on gold is reached. The O_2–O_2 sticking coefficient is calculated using data from 1000 s onwards. The average sticking coefficient (solid) gives the mean value of all sticking coefficients (dot-dashed) between time zero and time t. The inset graph (b) shows the original ion (*i.e.* molecule) count rate of the QMS during the O_2 gas exposure at room temperature and at 15.5 K. The hatched area marks the O_2-on-O_2-sticking zone.

spectrometer during the time of deposition and the gas load N_x^w at room temperature monitored over the same period of time as during the deposition. The sticking coefficient

$$S(T) = 1 - \frac{\int N_x^c \mathrm{d}t}{\int N_x^w \mathrm{d}t} \tag{3}$$

depends on the temperature and layer thickness. The results for O_2 and CO are summarized in Table 4 together with the N_2 values obtained previously. All sticking coefficients in Table 4 show lower limit values between 0.85 and 0.95 and thus are probably very close to unity.

Two main problems arise using this method. First, the molecules which do not hit the cryogenic surface can enter the QMS and cause an off-set in the signal level independent of the temperature of the sample surface. Thus, the given values are only lower limits to the true sticking coefficients. Second, the QMS has a response curve‡ which is a function of time, the examined species and the partial pressure regime itself. The response curve can be measured independently. Fig. 5b shows that the O_2 ion count of the QMS at room temperature peaks between 0 and 600 s even though a

‡ The iridium filament may be responsible for the QMS response curve since in general a QMS does not show this behavior. An alternative explanation for the ion current peak by assuming a hysteresis when opening the dosing valve can be excluded, because our pressure gauge does not see a peak pressure at the opening times at room temperature. Also, a hysteresis effect should not continue over 10 min.

constant flow is introduced to the system. For the estimate of the sticking coefficients a constant room temperature level at all times has been assumed (Fig. 5b, thin dashed line). When the sample is cooled down, lower partial pressures are measured during gas exposure and the filament response curve can be neglected. Thus the drop of the sticking coefficients of O_2 in Fig. 5a is not due to the room temperature peak between 0–1000 s but due to the difference of sticking probabilities between gold and oxygen.

The derivation of sticking coefficients between heterogeneous species S_{O_2-CO} like O_2 and CO is more difficult to estimate because only the short time at the beginning of the gas exposure before three or more monolayers are formed at cold temperatures can be used to measure S_{O_2-CO}. Due to the system response time a larger error applies to these early time measurements.

The tested molecules have not been pre-cooled and reached the cold surface with a kinetic energy around 300 K. If the incident molecule has less energy, *e.g.*, 100 K or 10 K as in interstellar space, the sticking coefficients of all examined species are expected to be higher than those at 300 K and thus can be assumed to be between 0.95 and 1.

4. Concluding remarks

The desorption and IR absorption behavior of $CO–O_2$ pure, mixed and layered ice systems has been investigated and compared to that of $CO–N_2$. The processes that are inferred from the experiments are schematically illustrated in Fig. 6. In contrast with $CO–N_2$, the morphology of the ices, *e.g.,* mixed or layered ices, does not strongly influence the desorption kinetics for the $CO–O_2$ ice system.

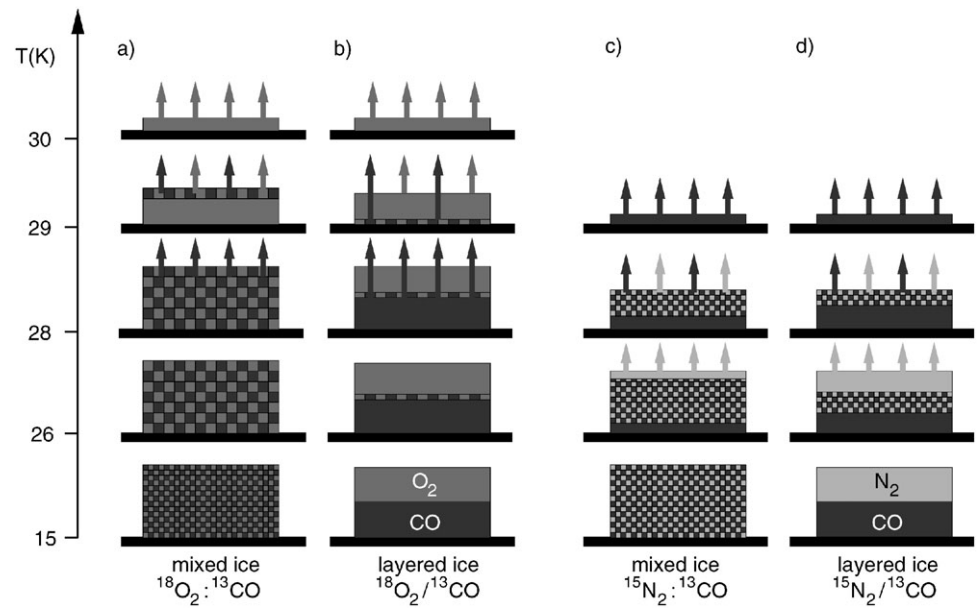

Fig. 6 Summary of different ice morphologies and their desorption behavior for $CO–O_2$ and $CO–N_2$ ice. Pure CO is represented by a dark grey area, N_2 by a light grey and O_2 by a solid grey area, whereas mixed ice regions are checkered. Desorption of a species is indicated by arrows of the corresponding grey scale. (a) In the mixed CO : O_2 ice a phase change of O_2 may occur around 25 K causing a partial segregation of CO and O_2 into microcrystals. Since CO is more volatile than O_2, desorption of CO in the CO : O_2 system first starts around 27–28 K. CO does not seem to codesorb with O_2. Thus, segregation of the CO : O_2 system happens *via* desorption at separate temperatures. At the end only O_2 is left in the $CO–O_2$ system. (b) The layered CO/O_2 ices show only weak mixing above 28 K. CO starts desorbing at 27–28 K. CO can desorb from underneath the O_2 layer without any difficulty. A small fraction of the remaining CO desorbs together with the main part of O_2 in the CO/O_2 ice. (c) Mixed CO : N_2 ices weakly segregate at temperatures higher than 20 K so that regions, *e.g.*, thin layers, of rather pure CO and N_2 are formed. Further heating above 25 K leads to the release of N_2 into the gas phase. At higher temperatures codesorption of N_2 with CO further depletes N_2 in the $CO–N_2$ system. Finally, only CO is left in the $CO–N_2$ system. (d) In the layered N_2/CO ice mixing occurs at temperatures above 20 K. At around 25–26 K, N_2 starts desorbing. At higher temperatures codesorption depletes the remaining N_2 and CO in the CO/N_2 system.

Under the current experimental conditions amorphous ices at low temperatures have been grown. At higher temperatures, *e.g.*, close to the desorption temperature, typical crystalline features appear in the RAIR spectra. In conclusion, the different behavior of O_2–CO and N_2–CO mixed and layered ices presented here both for TPD and RAIRS is explained by two structural physical differences: (1) N_2 and CO have the same α-phase crystalline structure at low temperatures whereas O_2 and CO have not, and (2) O_2 has a considerably lower quadrupole moment compared to N_2 which makes that interaction within the ice substantially weaker.

The desorption behavior of O_2, N_2 and CO can be included in astrochemical models by using the appropriate desorption mechanism. Heating rates of 1 K per 1000 years starting at 10 K can be considered typical conditions found near newly formed protostars.[38] Independent of the morphology of the ices, the desorption of N_2 and CO happens within 15–19 K, *i.e.* after 5000 to 9000 years.[2] O_2 desorbs between 18–20 K, *i.e.* after 8000–10 000 years.[25] A heating rate of 1 K per 10^6 yr or less is more relevant for pre-stellar cores and the expected temperature of O_2 desorption lies between 16–18 K (6–8 $\times$ 10^6 yr) and that of N_2 and CO at 13–17 K. The desorption of O_2 does not differ significantly between pure, layered and mixed ices and mainly follows a 0th-order desorption. Mixed and layered O_2 desorb at the same time or earlier than pure O_2. For N_2–CO ices this is different. Here, pure and mixed ices desorb in a single step where the desorption of mixed ices happens at higher temperatures, *i.e.* later times. For pure CO and N_2 ices a 0th-order desorption can be assumed and for the mixed ices a 1st-order desorption process. In general 0th-order desorption processes have a shorter desorption time than 1st-order processes. However, layered N_2 ices show a very pronounced codesorption and thus release the N_2 in a 2-step process into space. The size and height of this step depends on the amount of surface molecules and the diffusion process. From an astro-chemical point of view it is important to notice that O_2 desorbs at temperatures similar or higher than those of CO and N_2 and that the sticking coefficients of these molecules are all close to unity. This implies that solid O_2 could be a significant, but difficult to detect, reservoir of oxygen in cold clouds.

Our results demonstrate that the desorption of simple diatomic molecules can be rather complicated and that the underlying processes depend on structure as well as on the amount of molecules available. This confirms the results of Collings *et al.* and Kimmel *et al.* for simple systems containing H_2O[21,23] and shows that this kind of behavior is not an isolated effect but rather common for physisorbed systems.

Acknowledgements

We are grateful to Maria Palumbo and Otto Berg for their discussion concerning ^{13}CO spectra. Funding was provided by NOVA, FOM and a NWO Spinoza grant. K. A. would like to thank the Greenberg family for the Greenberg research fellowship and the ICSC-World Laboratory Fund.

References

1 K. I. Öberg, F. van Broekhuizen, H. J. Fraser , S. E. Bisscop, E. F. van Dishoeck and S. Schlemmer, *Astrophys. J. Lett.*, 2005, **621**, L33.
2 S. E. Bisschop, H. J. Fraser, K. I. Öberg, E. F. van Dishoeck and S. Schlemmer, *Astron. Astrophys.*, 2006, **449**, 1297.
3 E. A. Bergin, W. D. Langer and P. F. Goldsmith, *Astrophys. J.*, 1995, **441**, 222.
4 E. F. van Dishoeck, T. G. Phillips, J. Keene and G. A. Blake, *Astron. Astrophys.*, 1992, **261**, L13.
5 E. A. Bergin, J. Alves, T. Huard and C. J. Lada, *Astrophys. J. Lett.*, 2002, **570**, 101.
6 A. Belloche and P. André, *Astrophys. J.*, 2003, **593**, 906.
7 P. F. Goldsmith, G. J. Melnick, E. A. Bergin , J. E. Howe, R. L. Snell, D. A. Neufeld, M. Harwit, M. L. N. Ashby, B. M. Patten, S. C. Kleiner, R. Plume, J. R. Stauffer, V. Tolls, Z. Wang, Y. F. Zhang, N. R. Erickson, D. G. Koch, R. Schieder, G. Winnewisser and G. Chin, *Astrophys. J. Lett.*, 2000, **539**, L123.
8 L. Pagani, A. O. H. Olofsson, P. Bergman, P. Bernath, J. H. Black, R. S. Booth, V. Buat, J. Crovisier, C. L. Curry, P. J. Encrenaz, E. Falgarone, P. A. Feldman, M Fich, H. G. Floren, U. Frisk, M. Gerin, E. M. Gregersen, J. Harju, T. Hasegawa, Å. Hjalmarson, L. E. B. Johansson, S. Kwok, B. Larsson, A. Lecacheux, T. Liljeström, M. Lindqvist, R. Liseau, K. Mattila, G. F. Mitchell, L. H. Nordh, M. Olberg, G. Olofsson, I. Ristorcelli, Aa. Sandqvist, F. von Scheele, G. Serra, N. F. Tothill, K. Volk, T. Wiklind and C. D. Wilson, *Astron. Astrophys.*, 2003, **402**, L77.
9 R. Liseau and Odin Team, *Odin detection of O_2, Proc. IAU Symp. No. 231*, 2005.
10 K. M. Pontoppidan, PhD Thesis, Leiden University, 2004.

11 P. Ehrenfreund and E. van Dishoeck, *Adv. Space Res.*, 1998, **21**, 15.
12 T. I. Hasegawa, E. Herbst and C. M. Leung, *Astrophys. J., Suppl. Ser.*, 1992, **82**, 167.
13 A. G. G. M. Tielens and W. Hagen, *Astron. Astrophys.*, 1982, **114**, 245.
14 J. E. Chiar, P. A. Gerakines, D. C. B. Whittet, Y. J. Pendleton, A. G. G. M. Tielens, A. J. Adamson and A. C. A. Boogert, *Astrophys. J.*, 1998, **498**, 716.
15 K. M. Pontoppidan, H. J. Fraser, E. Dartois, W.-F. Thi, E. F. van Dishoeck, A. C. A. Boogert, L. d'Hendecourt, A. G. G. M. Tielens and S. E. Bisschop, *Astron. Astrophys.*, 2003, **408**, 981.
16 K. M. Pontoppidan, E. F. van Dishoeck and E. Dartois, *Astron. Astrophys.*, 2004, **426**, 925.
17 B. Vandenbussche, P. Ehrenfreund, A. C. A. Boogert, E. F. van Dishoeck, W. A. Schutte, P. A. Gerakines, J. Chiar, A. G. G. M. Tielens, J. Keane, D. C. B. Whittet, M. Breitfellner and M. Burgdorf, *Astron. Astrophys.*, 1999, **346**, L57.
18 P. Ehrenfreund, A. Boogert, P. Gerakines, A. Tielens and E. van Dishoeck, *Astron. Astrophys.*, 1997, **328**, 649.
19 J. Elsila, L. J. Allamandola and S. A. Sandford, *Astrophys. J.*, 1997, **479**, 818.
20 A. C. A. Boogert, G. A. Blake and A. G. G. M. Tielens, *Astrophys. J.*, 2002, **577**, 271.
21 G. A. Kimmel, K. P. Stevenson, Z. Dohnálek, R. S. Smith and B. D. Kay, *J. Chem. Phys.*, 2001, **114**, 5284.
22 H. J. Fraser, M. P. Collings, M. R. S. McCoustra and D. A. Williams, *Mon. Not. R. Astron. Soc.*, 2001, **327**, 1165.
23 M. Collings, J. Dever, H. Fraser and M. McCoustra, *Astrophys. J., Suppl. Ser.*, 2003, **285**, 633.
24 M. P. Collings, M. A. Anderson, R. Chen, J. W. Dever, S. Viti, D. A. Williams and M. R. S. McCoustra, *Mon. Not. R. Astron. Soc.*, 2004, **354**, 1133.
25 Acharyya *et al.*, in preparation, 2006.
26 F. A. van Broekhuizen, PhD Thesis, Leiden University, 2005.
27 J. C. Vickerman, *Surface Analysis: The Principle Techniques*, Wiley, New York, USA, 2004.
28 F. A. van Broekhuizen, I. M. N. Groot, H. J. Fraser, E. F. van Dishoeck and S. Schlemmer, Infrared spectroscopy of solid CO–CO_2 mixtures and layers, *Astron. Astrophys.*, 2005, accepted.
29 L. B. D'Hendecourt, L. J. Allamandola and J. M. Greenberg, *Astron. Astrophys.*, 1985, **152**, 130.
30 E. A. Bergin, G. J. Melnick, J. R. Stauffer, M. L. N. Ashby, G. Chin, N. R. Erickson, P. F. Goldsmith, M. Harwit, J. E. Howe, S. C. Kleiner, D. G. Koch, D. A. Neufeld, B. M. Patten, R. Plume, R. Schieder, R. L. Snell, V. Tolls, Z. Wang, G. Winnewisser and Y. F. Zhang, *Astrophys. J.*, 2000, **539**, L129.
31 G. Attard and C. Barnes, *Surfaces*, Oxford University Press, 1st edn, 1998.
32 G. Zumofen, *J. Chem. Phys.*, 1978, **68**, 3747.
33 H.-C. Chang, H. H. Richardson and G. E. Ewing, *J. Chem. Phys.*, 1988, **89**, 7561.
34 D. Fox and R. Hexter, *J. Chem. Phys.*, 1964, **41**, 1125.
35 M. E. Palumbo, G. A. Baratta, M. P. Collings and M. R. S. McCoustra, *Phys. Chem. Chem. Phys.*, 2005, **8**(2), 279.
36 Fuchs *et al.*, in preparation, 2006.
37 Acharyya *et al.*, in preparation, 2006.
38 J.-E. Lee, N. J. Evans and E. A. Bergin, *Astrophys. J.*, 2005, **631**, 351.
39 D. R. Lide, *CRC Handbook of Chemistry and Physics*, 82nd edn, CRC Press, Boca Raton, 2002.
40 V. G. Manzhelii and Y. A. Freiman, *Physics of Cryocrystals*, 1st edn, AIP Press, New York, USA, 1997.
41 Y. Freiman and H. Jodl, *Phys. Rep.*, 2004, **401**, 1.
42 D. E. Stogryn and A. P. Stogryn, *Mol. Phys.*, 1966, **11**, 371.